Improved efficiency critical-angle transmission gratings for high-resolution soft x-ray spectroscopy

Ralf K. Heilmann[a], Alexander R. Bruccoleri[b], Eric M. Gullikson[c], Hans Moritz Günther[d], Randall K. Smith[e], and Mark L. Schattenburg[a]

[a]Space Nanotechnology Laboratory, MIT Kavli Institute for Astrophysics and Space Research, Massachusetts Institute of Technology, Cambridge, MA 02139, USA
[b]Izentis, LLC, Cambridge, MA 02139, USA
[c]Lawrence Berkeley National Laboratory, Berkeley, CA 94720, USA
[d]MIT Kavli Institute for Astrophysics and Space Research, Massachusetts Institute of Technology, Cambridge, MA 02139, USA
[e]Center for Astrophysics, Harvard-Smithsonian Astrophysical Observatory, Cambridge, MA 02138, USA

ABSTRACT

High resolving power soft x-ray spectroscopy has been confirmed by the Astro2020 Decadal Survey as a high-priority strategic measurement technique with resolving power $R = \lambda/\Delta\lambda$ up to 7500 for some science cases. Examples are the characterization of highly ionized gases in galaxy halos and within and around galaxy clusters, accretion onto supermassive black holes, stellar coronal mass ejections and coronal heating. Arcus, a recently proposed high-resolution x-ray and FUV grating spectrometer Probe class mission, exceeds current capabilities by far, with a minimum R of 2500 ($\sim$ 3500 expected) and effective area up to 500 cm^2 in the 10-50 Å band, covered by the X-ray Spectrometer (XRS) instrument. The XRS relies on light-weight, high-efficiency, blazed and alignment-insensitive critical-angle transmission (CAT) gratings for dispersion and calls for hundreds of $\sim 30 \times 30$ mm^2 gratings. Recent gratings have been fabricated from 200-mm silicon-on-insulator (SOI) wafers using commercial tools from the semiconductor and MEMS industries compatible with volume production. Previously we reported x-ray results from quasi-fully illuminated co-aligned CAT gratings showing record-high R up to 1.3×10^4 in 18$^{\text{th}}$ and 21$^{\text{st}}$ diffraction orders at Al-K ($\sim$ 1.5 keV), and diffraction efficiency in agreement with synchrotron measurements and model predictions at O-K. We were recently able to chemically reduce the width of the freestanding, 200 nm-period, ultra-high aspect ratio CAT grating bars post-fabrication, and we report on the resulting increase in diffraction efficiency.

Keywords: Arcus, critical-angle transmission grating, x-ray spectroscopy, blazed transmission grating, soft x ray, grating spectrometer, high resolving power

1. INTRODUCTION

Apart from the movements of the moon and planets of our solar system the night sky looks mostly static. Visible changes on the time scale of a human observation are rare. With scientific equipment on the ground and aboard satellites we can see many changes in the brightness of objects, but movement outside of our solar system is still difficult to discern. However, our universe is a very dynamic place, and changes in position, temperature, density, abundance, magnetic fields and ionization states are primarily detected through spectroscopic measurements. While many imaging detectors have some intrinsic energy resolution, most are incapable of measuring the energy of the incident photons accurately and precisely enough to support sophisticated modeling of the physical conditions at the observed source. Instead, dedicated spectroscopic instruments are required. The Astro2020 Decadal Review, "Pathways to Discovery in Astronomy and Astrophysics"[1] states: "Astronomy became astrophysics with the first spectrum. Spectroscopy determines compositions, magnetic field strength, space motion, rotation,

Further author information: (Send correspondence to R.K.H.)
E-mail: ralf at space.mit.edu, URL: http://snl.mit.edu/

Space Telescopes and Instrumentation 2024: Ultraviolet to Gamma Ray, edited by Jan-Willem A. den Herder, Shouleh Nikzad, Kazuhiro Nakazawa, Proc. of SPIE Vol. 13093, 1309313
 · 0277-786X · doi: 10.1117/12.3020825

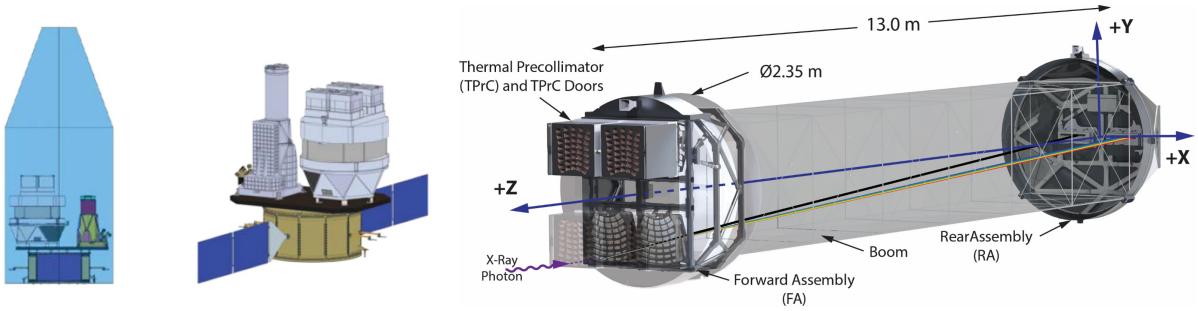

Figure 1. Arcus Probe schematics. Left: Spacecraft with instruments stowed in launch vehicle fairing. Middle: In space after solar panel deployment. The UV spectrometer is on the left, the XRS on the right. Right: XRS after boom deployment, showing the thermal precollimators and SPO arrays for the four OCs on the left. The grating petals are obscured behind the SPO arrays. An x ray is shown that enters the lower left OC and either lands at the telescope focus (black line) or gets diffracted into a blazed order (rainbow colors).

multiplicity, planetary companions, surface structure, and other important physical traits...In the next decade, spectroscopy will be the dominant discovery tool for astronomy."

The soft x-ray band, covering the characteristic lines of the most abundant "metals" (O, C, Ne, Fe, N, Si, Mg, S), is especially fertile ground for studying the composition and dynamics of the warm and hot, highly ionized plasmas that trace crucial feedback processes across up to fifteen orders of magnitude in size or distance. Examples of astrophysical subjects best studied with high-resolution soft x-ray spectroscopy are described in Refs. 2 and 3.

Arcus Probe is a proposed mission with two co-aligned high-resolution grating spectrometers: The X-ray Spectrometer (XRS) for the 1-5 nm band, and the Far UV Spectrograph (UVS)[4] for the 97-158 nm band (see Fig. 1). This paper concentrates on the XRS, which can deliver the desired spectra in much higher resolution and much shorter time than existing, aging[5,6] or new[7] soft x-ray observatories.

In the following we briefly describe the XRS and compare it to other x-ray spectroscopy missions. We briefly review CAT grating principles and fabrication, and then describe experiments for the thinning of CAT grating bars after fabrication. X-ray diffraction efficiency before and after thinning is compared before we summarize.

2. THE ARCUS PROBE X-RAY SPECTROMETER

The XRS features four parallel and nearly identical optical channels (OC). Each channel is a 12-m focal-length x-ray telescope, with a wedge-shaped sub-aperture of the NewAthena[8] silicon pore optics (SPO)[9] mirror array (see Fig. 1). Sub-aperturing creates an anisotropic telescope point-spread function (PSF).[10,11] Each mirror array is followed by a grating petal that holds 216 32×32.5 mm^2 critical-angle transmission (CAT) gratings. The gratings are arrayed and aligned along the surface of a tilted Rowland torus[12,13] and disperse along the narrow direction of the PSF, creating one linear spectrum per OC. The four quasi-parallel/antiparallel spectra - including the 0^{th} order - are read out with two shared CCD arrays.

CAT gratings are blazed transmission gratings. They consist of ultra-high aspect ratio, 200 nm-period, freestanding grating bars that are inclined by a small angle relative to the incident x rays. Diffracted orders around the direction of specular reflection from the nm-smooth sidewalls are strongly enhanced ("blazed"). This allows the use of higher orders than the Chandra[5,14] or XMM/Newton[6] grating spectrometers (which mostly operate in $\pm 1^{\text{st}}$ order) and thus leads to higher spectral resolving power. For example, $R \sim 1.3 \times 10^4$ has been demonstrated for an aligned pair of flight-like CAT gratings in 18^{th} order at Al-K wavelengths.[15]

The XRS combines the advantages of transmission and reflection grating-based instruments: relaxed alignment and stability tolerances, reduced part count due to near-normal incidence typical for transmission gratings, and higher diffraction efficiency and use of higher diffraction orders generally obtained with reflection gratings.

As a side benefit, CAT gratings become highly transparent at higher energies and thus are able to pass useful x rays (up to $\sim$ 10 keV in the case of the Arcus XRS) to a detector with its own intrinsic energy resolution

at the telescope focus. The left of Fig. 2 compares the expected zero order effective area for the Arcus XRS with existing missions, demonstrating that it is superior to Chandra and comparable to XMM-Newton in this regard. In addition, the PSF is significantly narrower than for XMM-Newton: it is anisotropic, with an expected FWHM < 3" in the dispersion direction, and < 9" in the cross dispersion direction. Although the signal will be at CCD resolution, this response will allow astronomers to confidently measure the high-energy continuum of sources such as stars, X-ray binaries, and AGN. Additionally, the response at 6-7 keV will allow measurement of Fe K features, which can then be correlated to features seen at Fe L, as, for example, in Ref. 16.

However, the XRS is primarily designed for optimum performance in the soft x-ray band ($\lambda > 10$ Å). The combination of CAT grating properties, sub-aperturing, and the compact and redundant design of the XRS leads to a very compelling instrument with figures of merit 1-2 orders of magnitude better than current spectrometers. See the right of Fig. 2 for an example.

The XRS is described in more detail in Refs. 17 and 18.

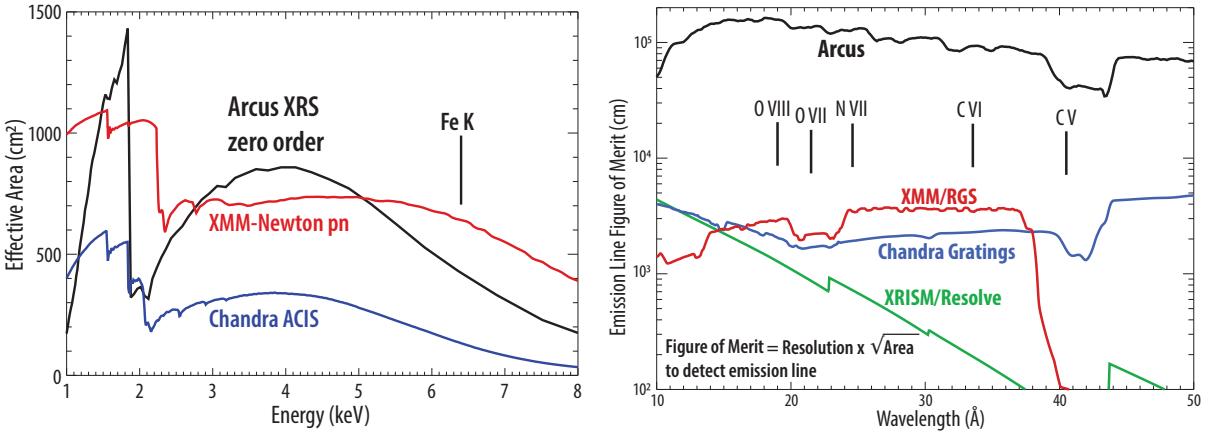

Figure 2. Left: Comparison of effective areas for imaging at x-ray energies in the 1-8 keV range. Despite being designed for high-resolution spectroscopy in the soft x-ray band, the Arcus XRS has the side-benefit of zero-order effective area similar to the XMM-Newton pn camera with CCD energy resolution of $\sim$ 70-100 eV. Right: Comparison of figure of merit for emission line detection between soft x-ray spectroscopy instruments in operation and the expected performance of the Arcus Probe XRS. "Chandra Gratings" refers to the better of HEG, MEG, and LETG. The curve for the Resolve microcalorimeter on XRISM[7] assumes that the closed aperture door is open. The wavelength ranges for important plasma diagnostics lines are also indicated.

3. CAT GRATINGS: OPERATING PRINCIPLE AND FABRICATION

CAT gratings feature ultra-high aspect-ratio, freestanding grating bars with nm-smooth sidewalls.[19] The entire grating is inclined such that x rays of wavelength λ impinge on the grating bar sidewalls at graze angles θ below the critical angle for total external reflection θ_c (see Fig. 3). The diffraction angle β_m for the m^{th} diffraction order is given by the grating equation

$$\frac{m\lambda}{p} = \sin\theta - \sin\beta_m, \tag{1}$$

where p is the grating period. Diffraction orders near the direction of specular reflection from the sidewalls show increased efficiency (i.e., blazing). The small critical angles for soft x rays (typically on the order of 1-2 degrees) demand high-aspect ratio grating bars in order to intercept all incoming photons. Furthermore, we want the bars to be as thin as possible to minimize blockage and absorption. We initially chose a design with grating period $p = 200$ nm, grating bar depth $d = 4$ micrometers, and bar thickness $b \approx 60$ nm. This is also the design baselined for Arcus. Recently we demonstrated $d > 5.5$ μm.[20] Blazing is most efficient when $\tan\theta \approx (p - b)/d$. (For $d = 4$ μm this means $\theta \approx 2$ deg.)

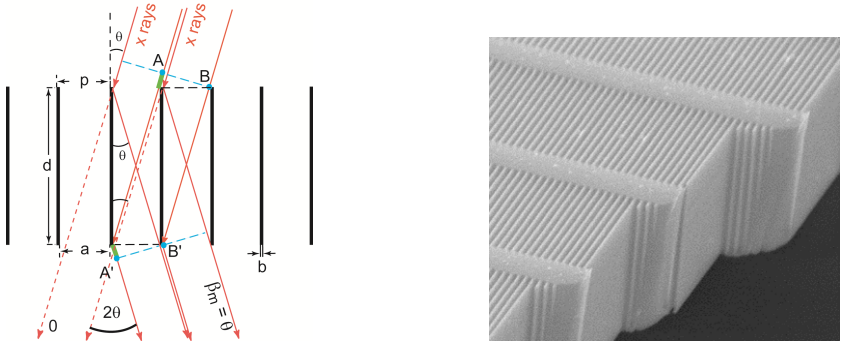

Figure 3. Left: Schematic cross-section through a CAT grating of period p. The m^{th} diffraction order occurs at an angle β_m where the path length difference between AA' and BB' is $m\lambda$. Shown is the case where β_m coincides with the direction of specular reflection from the grating bar sidewalls ($|\beta_m| = |\theta|$), i.e., blazing in the m^{th} order. Right: Scanning electron micrograph (SEM) of a cleaved CAT grating membrane showing top, cross-section and sidewall views of the 200 nm-period silicon grating bars and their monolithically integrated 5 μm-period L1 cross supports (x rays enter from the top and leave out the bottom).

CAT grating bars are not supported by a membrane, but freestanding. As seen on the right in Fig. 3, the bars are held in place by a monolithically integrated 5 μm-period Level 1 (L1) support mesh. Additional coarser and thicker support structures (Level 2/L2 hexagonal supports) are needed for the few-μm thin grating layer in order to manufacture large enough CAT gratings that can cover large areas on the order of thousands of square centimeters with a manageable number of gratings.

Fabrication has been described extensively in previous work.[19,21–23] CAT gratings are currently made from 200 mm silicon-on-insulator (SOI) wafers. The thin Si device ("front side") layer of the SOI wafer is manufactured to thickness d (see Fig. 3). Using 193 nm 4X optical projection lithography (OPL) at MIT Lincoln Laboratory, patterns for CAT gratings, L1 and L2 structures are simultaneously transferred into a silicon oxide layer that serves as a mask for the subsequent key step that creates the ultra-high aspect-ratio grating bars: the front side deep reactive-ion etch (DRIE). The ~ 0.6 mm thick handle ("back side") layer of the SOI wafer is then DRIE'd with a hexagonal pattern that is aligned with the front side L2 hexagons. The grating bars are aligned parallel to the vertical {111} planes of the (110) device layer. Since DRIE leaves rough sidewalls, this crystal orientation is used to "polish" the grating bar sidewalls post-DRIE through immersion in KOH solution.[19] The gratings have to be dried in a critical-point dryer to prevent stiction due to liquid-vapor surface tension. Finally, the buried oxide layer separating device and handle layers is removed in the areas not covered by Si, resulting in a monolithic Si grating layer with freestanding CAT grating bars, integrated L1 and L2 supports, and a bulky L2 mesh.

CAT gratings can be fabricated in volume manufacturing mode from 200 mm SOI wafers,[23] in principle allowing for $\sim 16 - 20$ gratings to be produced from a single wafer.

4. THINNING OF CAT GRATINGS AFTER FABRICATION

High diffraction efficiency requires efficient blazing, which in turn requires reflection from the sidewalls below the small critical angle for total external reflection. This requirement leads to the challenging ultra-high aspect ratio b/d (see Fig. 3). Concurrently, the bar width b should be as small as possible to minimize the blockage of incident x rays, while still preventing soft x rays from tunneling through the grating bars. Going below $b \sim 10 - 15$ nm would be counterproductive. At the same time there is a mechanical limit for grating bar width, below which the bars won't survive our current fabrication process, which involves a number of wet etching and cleaning steps that can lead to bubble formation and bar stiction due to surface tension effects.

Here we investigate an approach where the bars could be kept relatively wide throughout the current fabrication process, avoiding stiction, but are gently made thinner after the freestanding structure has been created.

4.1 Silicon Oxidation and Oxide Removal via Vapor HF Etching

The basic idea of thinning is simple: oxidation of Si will "consume" some Si during the formation of oxide. If we can then remove the oxide we are left with less Si than before, i.e., thinner grating bars.

In our experiments we simply let CAT gratings sit in the cleanroom air, which leads to the formation of a native oxide layer, typically 1-2 nm thick, on all exposed Si surfaces over 24 hours or less. However, the grating bars thicken less than twice the native oxide thickness, since obviously some of the Si gets "consumed" in the oxide formation. We then rest the grating structure over a hot HF solution and heat it from above with an IR lamp to prevent condensation. The HF vapor gently removes the silicon-containing oxide, leaving behind grating bars that are slightly narrower than before, even after regrowth of the native oxide. This process is repeated many times.

We take SEM images of the grating bars from the top after every ten cycles and estimate average values for b at the top of the bars from those images, with an estimated uncertainty of about 2-3 nm. This was first done on gratings etched into bulk Si[24] as a proof of concept. We have since repeated this experiment with three freestanding gratings that had their diffraction efficiency measured at a synchrotron beforehand.

Of the three tested gratings with $d \sim 6$ μm, one each underwent 10 (SP1), 20 (SP3) and 30 (SP5) cycles of HF vapor oxide removal and native oxide regrowth. (Deeper gratings with the same p have higher peak efficiency, but at smaller incidence angles. They are also more challenging to fabricate.) The oxide was allowed to reform for at least 24 hours before the next HF vapor etch. Fig. 4 shows top-down SEM images of grating SP3 before and after treatment. After image analysis we estimate the CAT grating bars to be $\sim 4 \pm 2$ nm thinner, changing from ~ 57 to ~ 53 nm at the top. Changes in thickness b deeper into the gratings obviously can not be discerned from SEM images. For grating SP1 we can not detect any clear changes. The changes for grating SP5 look similar to the ones for SP3.

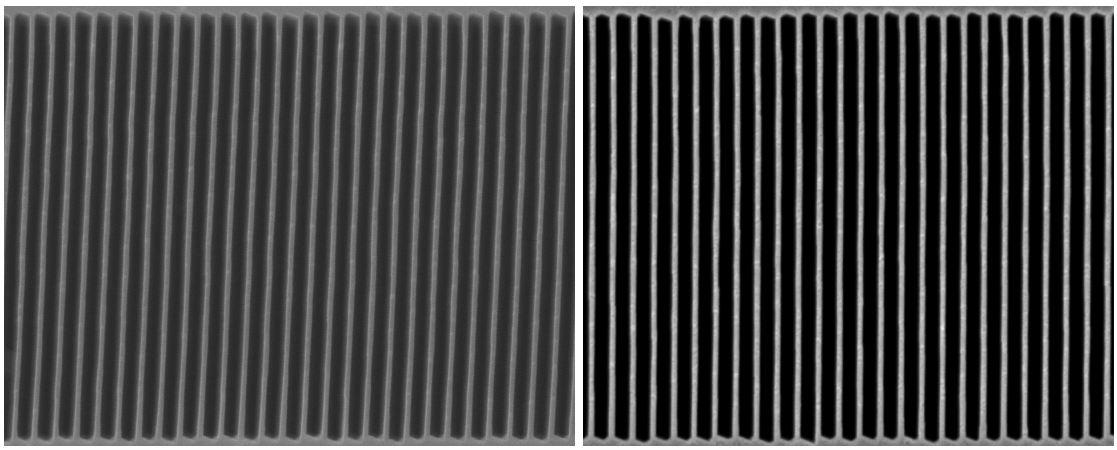

Figure 4. Top down scanning electron micrograph (SEM) images of grating SP3 before (left) and after 20 cycles of HF vapor etching and oxidation in ambient air (right). The 200 nm-period grating bars are slightly thinner after 20 cycles, but the difference is difficult to quantify precisely from SEM images alone.

4.2 X-ray Diffraction Efficiency Before and After Thinning

The gratings were measured for diffraction efficiency (DE) at the synchrotron eleven months after their initial synchrotron measurements, and about two months after the start of the HF vapor etching cycles. The gratings have a coarse hexagonal Level 3 (L3) support mesh with ~ 1 mm pitch. Measurements were taken with a sub-mm beam inside the same L3 hexagon as before on each sample, except for SP1, which unfortunately was damaged during handling in the area of the previously measured hexagon. For SP1 another hexagon near the original location was selected, and we could not discern a systematic increase or decrease of DE. For gratings SP3 and SP5 we show DE comparisons in Fig. 5. One can clearly see an increase in 0^{th} order efficiency, especially at normal incidence (angle = 0 deg.), which indicates less blockage by Si. For individual higher diffraction orders

the DE increase is less pronounced, but it is clearly visible when summing over the blazed orders. For both gratings we find an increase in blazed absolute efficiency in the range of 2-3% in the angular range where blazing is most efficient. Preliminary modeling of the DE with rigorous coupled-wave analysis[25] indicates that the CAT grating bars became $\sim$ 4-5 nm thinner on average, with average b approaching $\sim$ 42-44 nm. The data also show that DE is significantly higher than assumed for Arcus at this wavelength (see Fig. 6).

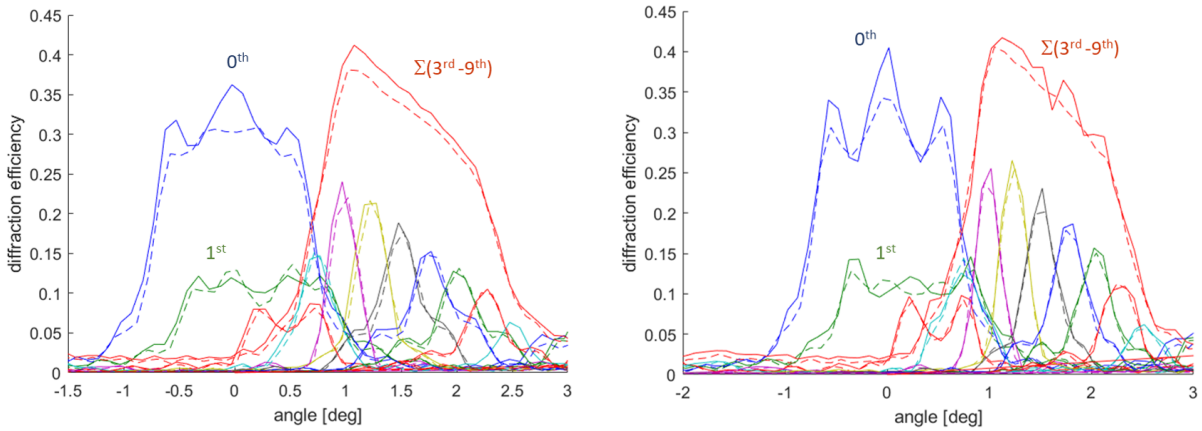

Figure 5. Measured diffraction efficiencies at $\lambda = 1.75$ nm for orders 0-10 and sum of orders 3-9 as a function of incidence angle. Dashed lines are before thinning, solid lines after thinning. Left: Grating SP3. Right: Grating SP5.

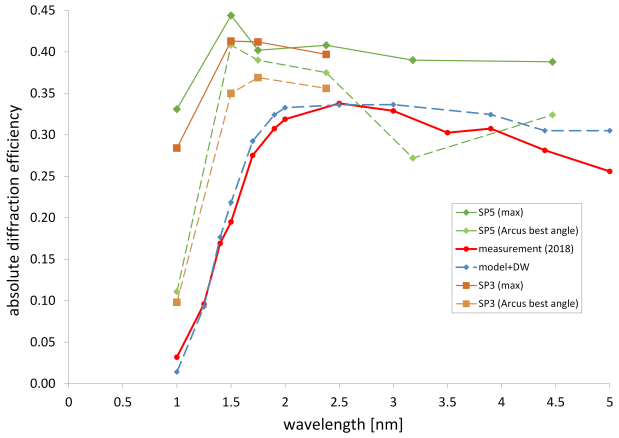

Figure 6. Diffraction efficiency (DE), including L1 blockage. "Model+DW" is the modelled DE for 4 μm deep CAT gratings with 16% L1 blockage, summed over the blazed orders that fall on the Arcus readouts. The red line is measured DE from 4 μm deep CAT gratings fabricated in 2017, summed over the same orders.[26] SP3 and SP5 are 6 μm deep gratings after thinning. "(Arcus best angle)" is the measured DE at the angle that gives the highest DE when summing over the orders that fall on the Arcus readouts, which have been designed for best blazing with 4 μm deep gratings. "(max)" is the measured DE summed over all blazed orders at the angle with the highest DE. The deeper gratings blaze optimally at smaller angles. Taking full advantage of the higher DE from deeper gratings would require a different layout for the readouts. Resolving power is reduced when utilizing diffraction orders at smaller angles.

While it is clear that HF vapor etching of silicon oxide leads to thinner grating bars, the etch could also change the roughness of the sidewalls, thereby increasing (lower roughness) or decreasing (higher roughness) DE. It is unclear why 10 treatment cycles seem to have caused little change, and why we see little difference in outcome between 20 and 30 etch/oxidation cycles. We plan to perform more systematic experiments, including fast growth of thicker oxide layers at elevated temperatures, to understand the different trade-offs between

experimental conditions and outcomes.

At the shorter wavelength of 1.0 nm the blaze condition is met for higher orders. At the same time, the critical angle for Si is only around 1.35 degrees, and blazing is reduced, especially at larger angles, due to the reduced sidewall reflectivity compared to 1.75 nm wavelength. As the sidewall reflectivity decreases with increasing incidence angle, more photons at this energy are able to penetrate the thin Si bars and end up in the 0^{th} order. The grating there behaves more like a phase-shifting transmission grating. Nevertheless, an increase in diffraction efficiency is still visible after thinning (see the left of Fig. 7). This seems to indicate that sidewall roughness has not increased substantially, because higher roughness would counteract higher throughput from thinning much more strongly for shorter wavelengths. As a side note, the 0^{th} order peaks at 1.9 degrees. At this angle ($\arctan p/d$) the Si density projected onto the incident x-ray wavefront is constant, and the grating acts like a low density Si film without useful diffraction.

At the longer wavelength of 2.38 nm we also observe increased 0^{th} order transmission after thinning, but the efficiency in the blazed orders appears to be relatively unchanged (see the right of Fig. 7). We speculate that this might be due to the fact that the produced grating bar profiles are not strictly rectangular, but typically seem to be narrower in the middle and wider at the top and bottom. At this wavelength Si is practically opaque, and diffraction within the narrow slots between grating bars takes place at larger angles. Any potential local reduced thinning could block these easily absorbed x rays and negate efficiency gains from thinning.

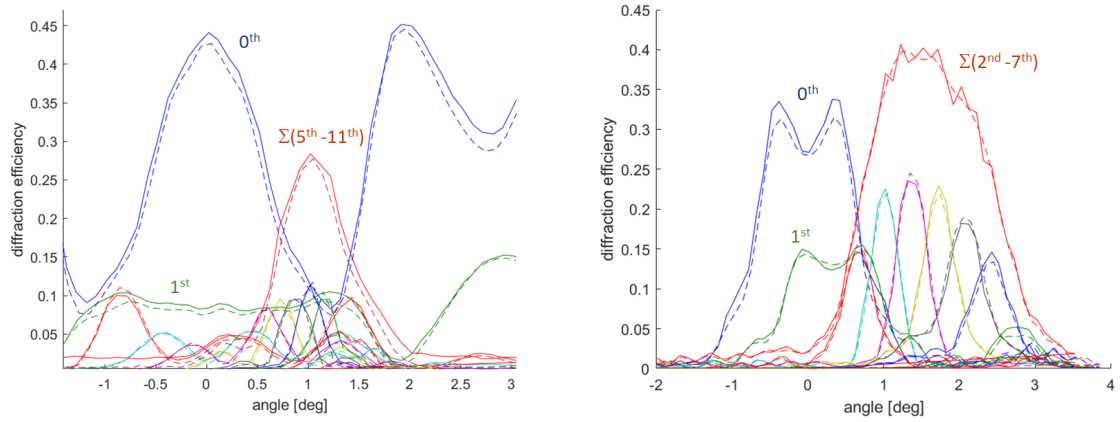

Figure 7. Left: Measured diffraction efficiencies at $\lambda = 1.0$ nm for orders 0-12 and sum of orders 5-11 as a function of incidence angle for grating SP3. Dashed lines are before thinning, solid lines after thinning. Right: Diffraction efficiencies at $\lambda = 2.38$ nm for orders 0-8 and sum of orders 2-7 as a function of incidence angle for grating SP5.

There will be a mechanical limit to making grating bars thinner, when the grating membrane could get damaged by launch vibrations. Vibration and temperature cycling testing so far have not revealed any problems,[26] but will have to be repeated for thinner and thinner structures.

5. DISCUSSION AND OUTLOOK

Arcus is a compelling mission, addressing high-priority science. Its high-resolution, CAT grating-based XRS will outperform existing soft x-ray spectroscopy instruments by orders of magnitude (see Fig. 2).

CAT gratings combine the advantages of x-ray transmission and reflection gratings. They have been under development for over a decade and perform in excess of Arcus requirements. However, to perform at the level envisioned for a next-generation Great X-ray Observatory such as Lynx,[27,28] more progress needs to be made, mostly in the area of diffraction efficiency or throughput and grating size.

In this article we have focused on thinning grating bars after the freestanding grating structure has been fabricated. The repeated application of room temperature oxidation and HF vapor oxide removal leads to thinner grating bars and improved diffraction efficiency. This proof-of-principle process is very gentle, but slow.

We plan to investigate faster oxidation at higher temperatures, where thicker oxide can be formed in a single step, and thinning by 10-20 nm might be achievable within hours instead of weeks.

Other obvious paths to higher throughput are support structures with less x-ray blockage,[29] also under investigation. The gratings from Section 4 all had L1 support bar widths of 1.1 μm, i.e., the L1 mesh had a duty cycle (DC) of 22%, which is wider than the intended 15% (the Arcus default) due to an easily correctable mask optical proximity effect. Most of our previously made gratings had lower DC around 15%, and we have fabricated CAT gratings with L1 DC of only 10%.[30] For most of the Arcus soft x-ray band the L1 bars are opaque, and therefore lower L1 DC directly translates into higher effective area for spectroscopy. In Fig. 6, going from 22 to 15% DC would lead to a relative increase in DE by 9% for gratings SP3 and SP5, for example.

The L2 hexagons currently have an open area fraction of 81%, which could be increased via changes in the OPL mask.

Larger gratings are expected to require less x-ray blocking area for mounting structures in a large grating array. One current problem for making larger gratings is the fact that our DRIE tools suffer from profile or bar tilt, i.e., the deep etched trenches are not all perpendicular to the substrate surface, but instead vary by many tenths of degrees over the surface of a wafer. Modern 200 mm DRIE tools perform better,[29] but tilt behavior can be fine-tuned if efficient metrology is available. Previously, we have used a combination of Small Angle X-ray Scattering and laser reflection to measure bar tilt, but this method is rather slow and labor intensive.[31] We are currently investigating Mueller Matrix Spectroscopic Ellipsometry (MMSE) as a fast, non-destructive method to measure bar tilt over a whole 200 mm wafer. Initial results will be published separately. If MMSE works as expected, it would enable immediate metrology feedback after the crucial front side DRIE step and speed up tuning of process parameters. In production it would serve as a valuable control to keep process parameters from drifting.

ACKNOWLEDGMENTS

We thank J. Gregory, D. Young, and R. Lambert (MIT Lincoln Lab) for OPL and front side mask patterning of 200 mm SOI wafers. We gratefully acknowledge facility support from MIT.nano. This work was supported by NASA grants 80NSSC20K0780 and 80NSSC22K1904, and by the MIT Kavli Institute for Astrophysics and Space Research. A part of this work used resources of the Advanced Light Source, which is a DOE Office of Science User Facility under contract no. DE-AC02-05CH11231. Some of the material presented in this proceedings paper has been submitted for publication to the Journal of Astronomical Telescopes, Instruments, and Systems.[17]

REFERENCES

[1] National Academies of Sciences, Engineering, and Medicine, "Pathways to Discovery in Astronomy and Astrophysics for the 2020s," (2021).

[2] Smith, R. K., Bautz, M., Bregman, J., Brenneman, L., Brickhouse, N., Bulbul, E., Burwitz, V., Bushman, J., Canizares, C., Chakrabarty, D., Cheimets, P., Costantini, E., DeRoo, C., Falcone, A., Foster, A., Gallo, L., Grant, C., Guenther, H. M., Heilmann, R. K., Heine, S., Hine, B., Huenemoerder, D., Jara, S., Kaastra, J., Kara, E., Kreykenbohm, I., Madsen, K., Marshall, H., McDonald, M., McEntaffer, R., Miller, J., Miller, E., Mushotzky, R., Nandra, K., Nowak, M., Paerels, F., Petre, R., Poppenhaeger, K., Ptak, A., Reid, P., Ronzano, K., Rozanska, A., Samra, J., Sanders, J., Schattenburg, M., Schonfeld, J., Schulz, N., Smale, A., Temi, P., Valencic, L., Walker, S., Wilms, J., and Wolk, S., "Arcus: exploring the formation and evolution of clusters, galaxies, and stars," in [*Space Telescopes and Instrumentation 2022: Ultraviolet to Gamma Ray*], den Herder, J.-W. A., Nikzad, S., and Nakazawa, K., eds., **12181**, 1218121, International Society for Optics and Photonics, SPIE (2022).

[3] Smith, R. K., "The Arcus Probe mission," in [*UV, X-Ray, and Gamma-Ray Space Instrumentation for Astronomy XXIII*], **12678**, International Society for Optics and Photonics, SPIE (2023).

[4] Fleming, B. T., France, K., Patton, T., Hellickson, T., Nell, N., Smith, R., and Cheimets, P., "The Arcus ultraviolet spectrograph (UVS): technical design of the far-ultraviolet spectrograph on the Arcus probe," in [*UV, X-Ray, and Gamma-Ray Space Instrumentation for Astronomy XXIII*], Siegmund, O. H. and Hoadley, K., eds., **12678**, 126780G, International Society for Optics and Photonics, SPIE (2023).

[5] Canizares, C., Davis, J., Dewey, D., Flanagan, K., Galton, E., Huenemoerder, D., Ishibashi, K., Markert, T., Marshall, H., McGuirk, M., Schattenburg, M., Schulz, N., Smith, H., and Wise, M., "The Chandra high-energy transmission grating: Design, fabrication, ground calibration, and 5 years in flight," *PUBLICATIONS OF THE ASTRONOMICAL SOCIETY OF THE PACIFIC* **117**, 1144–1171 (OCT 2005).

[6] den Herder, J., Brinkman, A., Kahn, S., Branduardi-Raymont, G., Thomsen, K., Aarts, H., Audard, M., Bixler, J., den Boggende, A., Cottam, J., Decker, T., Dubbeldam, L., Erd, C., Goulooze, H., Gudel, M., Guttridge, P., Hailey, C., Al Janabi, K., Kaastra, J., de Korte, P., van Leeuwen, B., Mauche, C., McCalden, A., Mewe, R., Naber, A., Paerels, F., Peterson, J., Rasmussen, A., Rees, K., Sakelliou, I., Sako, M., Spodek, J., Stern, M., Tamura, T., Tandy, J., de Vries, C., Welch, S., and Zehnder, A., "The reflection grating spectrometer on board XMM-Newton," *ASTRONOMY & ASTROPHYSICS* **365**, L7–L17 (JAN 2001).

[7] Ishisaki, Y., Kelley, R. L., Awaki, H., Balleza, J. C., Barnstable, K. R., Bialas, T. G., Boissay-Malaquin, R., Brown, G. V., Canavan, E. R., Cumbee, R. S., Carnahan, T. M., Chiao, M. P., Comber, B. J., Costantini, E., den Herder, J.-W., Dercksen, J., de Vries, C. P., DiPirro, M. J., Eckart, M. E., Ezoe, Y., Ferrigno, C., Fujimoto, R., Gorter, N., Graham, S. M., Grim, M., Hartz, L. S., Hayakawa, R., Hayashi, T., Hell, N., Hoshino, A., Ichinohe, Y., Ishida, M., Ishikawa, K., James, B. L., Kenyon, S. J., Kilbourne, C. A., Kimball, M. O., Kitamoto, S., Leutenegger, M. A., Maeda, Y., McCammon, D., Miko, J. J., Mizumoto, M., Okajima, T., Okamoto, A., Paltani, S., Porter, F. S., Sato, K., Sato, T., Sawada, M., Shinozaki, K., Shipman, R., Shirron, P. J., Sneiderman, G. A., Soong, Y., Szymkiewicz, R., Szymkowiak, A. E., Takei, Y., Tamura, K., Tsujimoto, M., Uchida, Y., Wasserzug, S., Witthoeft, M. C., Wolfs, R., Yamada, S., and Yasuda, S., "Status of Resolve instrument onboard X-Ray Imaging and Spectroscopy Mission (XRISM)," in [*Space Telescopes and Instrumentation 2022: Ultraviolet to Gamma Ray*], den Herder, J.-W. A., Nikzad, S., and Nakazawa, K., eds., **12181**, 121811S, International Society for Optics and Photonics, SPIE (2022).

[8] Bavdaz, M., Wille, E., Ayre, M., Ferreira, I., Shortt, B., Fransen, S., Collon, M. J., Vacanti, G., Barrière, N. M., Landgraf, B., Girou, D., Riekering, M. O., Haneveld, J., Start, R., Schurink, B., van Baren, C., Ferreira, D. D. M., Massahi, S., Svendsen, S., Christensen, F., Krumrey, M., Skroblin, D., Burwitz, V., Pareschi, G., Salmaso, B., Moretti, A., Spiga, D., Basso, S., Valsecchi, G., Vernani, D., Lupton, P., Mundon, W., Dunnell, E., Riede, M., Korhonen, T., Pasanen, M., Sanchez, A., Heinis, D., Colldelram, C., Tordi, M., Niewrzella, N., and Willingale, R., "NewATHENA optics technology," in [*Optics for EUV, X-Ray, and Gamma-Ray Astronomy XI*], O'Dell, S. L., Gaskin, J. A., Pareschi, G., and Spiga, D., eds., **12679**, 1267902, International Society for Optics and Photonics, SPIE (2023).

[9] Landgraf, B., Abalo, L., Barrière, N. M., Bayerle, A., de Borst, D., Castiglione, L., Collon, M. J., Crama, L., Chatbi, A., Eenkhoorn, N., Girou, D., Günther, R., Hauser, E., van der Hoeven, R., den Hollander, J., Jenkins, Y., Lassise, A., Keek, L., Körnig, C., Obwaller, S., Okma, B., da Silva Ribeiro, P., Rizos, C., Thete, A., Vacanti, G., Verhoeckx, S., Vervest, M., Visser, R., Voruz, L., Bavdaz, M., Wille, E., Ferreira, I., Bosman, M., Haneveld, J., Koelewijn, A., Lankwarden, J.-J., Riekerink, M. O., Schurink, B., Start, R., Wijnperle, M., van Baren, C., Cibik, L., Krumrey, M., Skroblin, D., Burwitz, V., Christensen, F. E., Ferreira, D. D. M., Massahi, S., Sanz, D. P., Svendsen, S., Dunnell, E., Lupton, P., Mundon, W., Rees, A., and Watley, D., "High-resolution and light-weight silicon pore x-ray optics," in [*Optics for EUV, X-Ray, and Gamma-Ray Astronomy XI*], O'Dell, S. L., Gaskin, J. A., Pareschi, G., and Spiga, D., eds., **12679**, 1267903, International Society for Optics and Photonics, SPIE (2023).

[10] Cash, W., "X-ray optics .2. a technique for high-resolution spectroscopy," *APPLIED OPTICS* **30**, 1749–1759 (MAY 1 1991).

[11] Heilmann, R. K., Davis, J. E., Dewey, D., Bautz, M. W., Foster, R., Bruccoleri, A., Mukherjee, P., Robinson, D., Huenemoerder, D. P., Marshall, H. L., Schattenburg, M. L., Schulz, N. S., Guo, L. J., Kaplan, A. F., and Schweikart, R. B., "Critical-angle transmission grating spectrometer for high-resolution soft x-ray spectroscopy on the International X-ray Observatory," in [*SPACE TELESCOPES AND INSTRUMENTATION 2010: ULTRAVIOLET TO GAMMA RAY*], Arnaud, M., Murray, S., and Takahashi, T., eds., *Proceedings of SPIE* **7732**, SPIE (2010). Conference on Space Telescopes and Instrumentation 2010 - Ultraviolet to Gamma Ray, San Diego, CA, JUN 28-JUL 02, 2010.

[12] Günther, H. M., Cheimets, P. N., Heilmann, R. K., Smith, R. K., and Collaboration, A., "Performance of a double tilted-Rowland-spectrometer on Arcus," in [*UV, X-RAY, AND GAMMA-RAY SPACE INSTRUMENTATION FOR ASTRONOMY XX*], Siegmund, O., ed., *Proceedings of SPIE* **10397**, SPIE (2017).

Conference on UV, X-Ray, and Gamma-Ray Space Instrumentation for Astronomy XX, San Diego, CA, AUG 06-08, 2017.

[13] Günther, H. M., DeRoo, C., Heilmann, R. K., and Hertz, E., "Concept of a double tilted Rowland spectrograph for x-rays," submitted to ApJ (2024).

[14] Predehl, P., Kraus, H., Braeuninger, H. W., Burkert, W., Kettenring, G., and Lochbihler, H., "Grating elements for the AXAF low-energy transmission grating spectrometer," in [*EUV, X-Ray, and Gamma-Ray Instrumentation for Astronomy III*], **1743**, 475–481, SPIE (Oct. 1992).

[15] Heilmann, R. K., Bruccoleri, A. R., Burwitz, V., deRoo, C., Garner, A., Günther, H. M., Gullikson, E. M., Hartner, G., Hertz, E., Langmeier, A., Müller, T., Rukdee, S., Schmidt, T., Smith, R. K., and Schattenburg, M. L., "X-ray performance of critical-angle transmission grating prototypes for the Arcus mission," *ASTROPHYSICAL JOURNAL* **934** (2022).

[16] Zoghbi, A., Fabian, A. C., Uttley, P., Miniutti, G., Gallo, L. C., Reynolds, C. S., Miller, J. M., and Ponti, G., "Broad iron L line and X-ray reverberation in 1H0707-495," *Monthly Notices of the Royal Astronomical Society* **401**, 2419–2432 (01 2010).

[17] Heilmann, R. K., Bruccoleri, A. R., Gregory, J. A., Gullikson, E. M., Günther, H. M., Hertz, E., Lambert, R. D., Young, D. J., and Schattenburg, M. L., "Transmission grating arrays for the x-ray spectrometer on Arcus Probe," submitted to JOURNAL OF ASTRONOMICAL TELESCOPES INSTRUMENTS AND SYSTEMS (2024).

[18] Günther, H. M. and Heilmann, R. K., "Arcus x-ray telescope performance predictions and alignment requirements," submitted to JOURNAL OF ASTRONOMICAL TELESCOPES INSTRUMENTS AND SYSTEMS (2024).

[19] Bruccoleri, A., Guan, D., Mukherjee, P., Heilmann, R. K., Schattenburg, M. L., and Vargo, S., "Potassium hydroxide polishing of nanoscale deep reactive-ion etched ultrahigh aspect ratio gratings," *JOURNAL OF VACUUM SCIENCE & TECHNOLOGY B* **31** (NOV 2013).

[20] Heilmann, R. K., Bruccoleri, A. R., Song, J., Levenson, B., Smallshaw, B., Whalen, M., Garner, A., Heine, S. T., Marshall, H. L., Cook, M. T., Gregory, J. A., Lambert, R. D., Shapiro, D. A., Young, D. J., Gullikson, E. M., Nonaka, T., Uchida, A., Quijada, M. A., Hertz, E., Cheimets, P., Smith, R. K., and Schattenburg, M. L., "Manufacture and performance of blazed soft x-ray transmission gratings for Arcus and Lynx," in [*OPTICS FOR EUV, X-RAY, AND GAMMA-RAY ASTRONOMY X*], ODell, S., Gaskin, J., and Pareschi, G., eds., *Proceedings of SPIE* **11822**, SPIE (2021). Conference on Optics for EUV, X-Ray, and Gamma-Ray Astronomy X, San Diego, CA, AUG 01-05, 2021.

[21] Bruccoleri, A. R., Guan, D., Heilmann, R. K., Vargo, S., DiPiazza, F., and Schattenburg, M. L., "Nanofabrication advances for high efficiency critical-angle transmission gratings," in [*OPTICS FOR EUV, X-RAY, AND GAMMA-RAY ASTRONOMY VI*], ODell, S. and Pareschi, G., eds., *Proceedings of SPIE* **8861**, SPIE (2013). Conference on Optics for EUV, X-Ray, and Gamma-Ray Astronomy VI as part of the SPIE Optics + Photonics International Symposium on Optical Engineering + Applications, San Diego, CA, AUG 26-29, 2013.

[22] Bruccoleri, A. R., Heilmann, R. K., and Schattenburg, M. L., "Fabrication process for 200 nm-pitch polished freestanding ultrahigh aspect ratio gratings," *JOURNAL OF VACUUM SCIENCE & TECHNOLOGY B* **34** (NOV-DEC 2016).

[23] Heilmann, R. K., Bruccoleri, A. R., Song, J., Cook, M. T., Gregory, J. A., Lambert, R. D., Shapiro, D. A., Young, D. J., Bradshaw, M., Burwitz, V., Hartner, G. D., Langmeier, A., Smith, R. K., and Schattenburg, M. L., "Toward volume manufacturing of high-performance soft x-ray critical-angle transmission gratings," in [*SPACE TELESCOPES AND INSTRUMENTATION 2020: ULTRAVIOLET TO GAMMA RAY*], Den-Herder, J., Nikzad, S., and Nakazawa, K., eds., *Proceedings of SPIE* **11444**, SPIE (2021). Conference on Space Telescopes and Instrumentation - Ultraviolet to Gamma Ray / SPIE Astronomical Telescopes + Instrumentation Conference, DEC 14-18, 2020.

[24] Heilmann, R. K., Bruccoleri, A. R., Burwitz, V., Cheimets, P., DeRoo, C., Garner, A., Gullikson, E. M., Günther, H. M., Hartner, G., Hertz, E., Langmeier, A., Mueller, T., Rukdee, S., Schmidt, T., Smith, R. K., and Schattenburg, M. L., "Flight-like critical-angle transmission grating x-ray performance for Arcus," in [*Space Telescopes and Instrumentation 2022: Ultraviolet to Gamma Ray*], den Herder, J.-W. A., Nikzad, S., and Nakazawa, K., eds., **12181**, 1218116, International Society for Optics and Photonics, SPIE (2022).

[25] Moharam, M., Pommet, D., Grann, E., and Gaylord, T., "Stable implementation of the rigorous coupled-wave analysis for surface-relief gratings - enhanced transmittance matrix approach," *JOURNAL OF THE OPTICAL SOCIETY OF AMERICA A-OPTICS IMAGE SCIENCE AND VISION* **12**, 1077–1086 (MAY 1995). Optical-Society-of-America 2nd Topical Meeting on Diffractive Optics, ROCHESTER, NY, JUN 06-09, 1994.

[26] Heilmann, R. K., Bruccoleri, A. R., Song, J., Kolodziejczak, J., Gaskin, J. A., O'Dell, S. L., Cheimetz, P., Hertz, E., Smith, R. K., Burwitz, V., Hartner, G., La Caria, M.-M., and Schattenburg, M. L., "Critical-angle transmission grating technology development for high resolving power soft x-ray spectrometers on Arcus and Lynx," in [*OPTICS FOR EUV, X-RAY, AND GAMMA-RAY ASTRONOMY VIII*], ODell, S. and Pareschi, G., eds., *Proceedings of SPIE* **10399**, SPIE (2017). Conference on Optics for EUV, X-Ray, and Gamma-Ray Astronomy VIII, San Diego, CA, AUG 08-10, 2017.

[27] Gaskin, J. A., Swartz, D. A., Vikhlinin, A., Ozel, F., Gelmis, K. E., Arenberg, J. W., Bandler, S. R., Bautz, M. W., Civitani, M. M., Dominguez, A., Eckart, M. E., Falcone, A. D., Figueroa-Feliciano, E., Freeman, M. D., Guenther, H. M., Havey, K. A., Heilmann, R. K., Kilaru, K., Kraft, R. P., McCarley, K. S., McEntaffer, R. L., Pareschi, G., Purcell, W., Reid, P. B., Schattenburg, M. L., Schwartz, D. A., Schwartz, E. D., Tananbaum, H. D., Tremblay, G. R., Zhang, W. W., and Zuhone, J. A., "Lynx x-ray observatory: an overview," *JOURNAL OF ASTRONOMICAL TELESCOPES INSTRUMENTS AND SYSTEMS* **5** (APR 2019).

[28] Güenther, H. M. and Heilmann, R. K., "Lynx soft x-ray critical-angle transmission grating spectrometer," *JOURNAL OF ASTRONOMICAL TELESCOPES INSTRUMENTS AND SYSTEMS* **5** (APR 2019).

[29] Heilmann, R. K., Bruccoleri, A. R., Gullikson, E. M., Smith, R. K., and Schattenburg, M. L., "Soft x-ray performance and fabrication of flight-like blazed transmission gratings for the x-ray spectrometer on Arcus Probe," in [*Optics for EUV, X-Ray, and Gamma-Ray Astronomy XI*], O'Dell, S. L., Gaskin, J. A., Pareschi, G., and Spiga, D., eds., **12679**, 126790L, International Society for Optics and Photonics, SPIE (2023).

[30] Heilmann, R. K., Bruccoleri, A. R., Song, J., and Schattenburg, M. L., "Progress in x-ray critical-angle transmission grating technology development," in [*OPTICS FOR EUV, X-RAY, AND GAMMA-RAY ASTRONOMY IX*], ODell, S. and Pareschi, G., eds., *Proceedings of SPIE* **11119**, SPIE (2019). Conference on Optics for EUV, X-Ray, and Gamma-Ray Astronomy IX as part of the SPIE Optics + Photonics International Symposium on Optical Engineering + Applications, San Diego, CA, AUG 13-15, 2019.

[31] Song, J., Heilmann, R. K., Bruccoleri, A. R., and Schattenburg, M. L., "Characterizing profile tilt of nanoscale deep-etched gratings via x-ray diffraction," *JOURNAL OF VACUUM SCIENCE & TECHNOLOGY B* **37** (NOV 2019).